Applied Catalysis B: Environmental 320 (2023) 121982

Contents lists available at ScienceDirect

Applied Catalysis B: Environmental

journal homepage: www.elsevier.com/locate/apcatb

Revealing hydrogen migration effect on ammonia synthesis activity over ceria-supported Ru catalysts

Chunyan Li, Minghui Li, Yiping Zheng, Biyun Fang, Jianxin Lin, Jun Ni *, Bingyu Lin *, Lilong Jiang *

National Engineering Research Center of Chemical Fertilizer Catalyst, College of Chemical Engineering, Fuzhou University, Fuzhou 350002, Fujian, China

ARTICLE INFO

Keywords:
Hydrogen migration
Metal–support interactions
Ceria
Ru catalyst
Ammonia synthesis

ABSTRACT

Catalytic reactions involving hydrogen over reducible oxide-supported metal catalysts are inseparable from the hydrogen storage capacity and hydrogen migration, which are mainly dependent on the interaction between reducible oxides and active metals. In this work, we report that the hydrogen migration rate of Ru/CeO_2 could be tuned by changing cerium nitrate solvents for the preparation of ceria. There are more kinds of oxygen species and a large amount of Ce^{3+} concentration, defects and Ru–O–Ce interfacial sites for Ru catalyst supported on ceria obtained by ethanol-precipitated synthesis, resulting in a reduction in the amount of the exposed Ru species and proportion of Ru metal. In such a case, the migration and desorption of hydrogen species as well as nitrogen activation would be inhibited. Conversely, there are a higher ratio of Ru metal and a great deal of the Ru exposure for Ru catalyst supported on ceria obtained by water-precipitated synthesis, facilitating the migration and desorption of hydrogen species, as well as nitrogen activation. As a result, the water-precipitated synthesized ceria-supported Ru catalyst has 4.9-fold higher in catalytic activity than Ru catalyst supported on the ethanol-precipitated synthesized ceria. This work provides insight into the design of Ru catalysts used ammonia synthesis by controlling hydrogen spillover and migration between Ru species and CeO_2.

1. Introduction

Ammonia, as the support of modern civilization, has largely pushed forward the progress of human society due to its intensive application [1,2]. In recent years, researchers are devoted to the development and application of the renewable energy, and ammonia is one of the most perspective candidates as a hydrogen energy carrier or a carbon-free fuel because of its high hydrogen content and energy density [3,4]. It is indisputable that ammonia production based on Haber–Bosch process [5,6] using iron catalysts greatly affects society and civilization. However, under the circumstance of energy shortage and environment crisis, the high energy consumption as well as carbon emission originated from Haber–Bosch process should not be ignored [1,7,8]. Consequently, the development of a higher efficient catalyst for NH_3 synthesis under mild condition is the priority for researchers.

Ru catalyst supported on carbon is the second generation ammonia synthesis catalyst following Fe-based catalysts because of the substantial reduce of the energy consumption in ammonia synthesis [9]. Unfortunately, the deactivation problem of Ru/C catalyst limits its further industrial application, and efforts on the replacement of carbon with oxides are going. Actually, Ru/CeO_2 catalysts have caught attention in ammonia synthesis because CeO_2 has good H_2 storage capacity, adequate surface defects, electronic properties and redox potential between Ce^{3+} and Ce^{4+} cations [10–14]. In such cases, the ammonia synthesis performances of Ru catalysts supported on ceria can be improved by the appropriate tuning of the properties of ceria. For example, Ma et al. found that the change in CeO_2 morphology affected the ammonia synthesis activity of Ru/CeO_2 by changing the surface composition/electronic structure and exposed crystal planes of ceria [11]. Lin et al. proposed that the difference in CeO_2 morphology resulted in the changes of Ru particle sizes, the existing states and quantity of oxygen vacancies, leading to the variation of the hydrogen desorption pathway and the ammonia synthesis activity [12]. Li et al. claimed that the introduction of Ti into ceria resulted in the decrease of the quantity of the active oxygen by forming a $CeTiO_x$ solid solution, which strongly affected the ammonia synthesis rates by modulating the adsorption property of ceria-supported Ru catalyst [13,14].

The defects in CeO_2 not only play a crucial role in the existing form

* Corresponding authors.
E-mail addresses: nj@fzu.edu.cn (J. Ni), bylin@fzu.edu.cn (B. Lin), jll@fzu.edu.cn (L. Jiang).

https://doi.org/10.1016/j.apcatb.2022.121982
Received 28 June 2022; Received in revised form 6 September 2022; Accepted 12 September 2022
Available online 13 September 2022

and the desorption pathway of hydrogen species, but also affect the reactivity of surface hydroxyl groups [15]. There is a hydrogen spillover phenomenon over ceria-supported Ru catalysts [16–19], that is, hydrogen molecule would adsorb and dissociate on Ru metal, and then migrate into ceria support. This phenomenon also would be found for various metal catalysts supported on TiO_2 or other reducible oxides [20, 21]. The spillover can effectively increase the hydrogen storage capacities for reducible oxide-supported metal catalysts. However, the migration rate of hydrogen species might also play a crucial role in the catalytic performances of the hydrogen-involved reactions. Ammonia synthesis is a hydrogen-involving reaction that requires metallic Ru as active sites, and Li et al. suggested that N_2H_4 reduction or $NaBH_4$ treatment of Ru/CeO_2 catalysts facilitated hydrogen spillover from the catalyst surface, leading to an improvement of NH_3 synthesis activities [22,23]. Mao et al. proposed that the hydrogen spillover from Fe to oxygen vacancies leaded to the formation of O_V-H, contributing to break the scaling relationship of ammonia synthesis and thus the performance of ammonia synthesis for $TiO_{2-x}H_y$/Fe would be enhanced significantly [24]. It can be envisaged that the ammonia synthesis activity would be enhanced by an appropriately tuning hydrogen spillover of Ru/CeO_2 catalyst, however, the effect of hydrogen migration on the ammonia synthesis activity is not well understood and the optimal Ru/CeO_2 catalyst is yet to be obtained. In this work, two ceria are prepared by water-precipitated synthesis and ethanol-precipitated synthesis, respectively, and the resulting samples are used as support materials of Ru catalysts. There are no significant differences in electronic metal−support interaction between Ru and ceria for Ru catalysts. However, a larger amount of the exposed Ru species and a higher proportion of metallic Ru would be detected over Ru catalyst supported on ceria obtained by water-precipitated synthesis, leading to enhancement of ammonia synthesis activities by boosting hydrogen migration and desorption as well as nitrogen activation. Conversely, the sample with ceria support prepared by the ethanol-precipitated synthesis has more kinds of oxygen species and larger number of Ru−O−Ce interfacial sites, defects and Ce^{3+} concentration, resulting in the lowering of hydrogen migration as well as catalytic performances. This result shows that the change in cerium nitrate solvents for the preparation of ceria strongly affects the hydrogen migration and desorption of Ru/CeO_2 catalysts, which is crucial to ammonia synthesis.

2. Experimental section

2.1. Catalyst preparation

CeO_2-e was prepared by precipitation method using ethanol as solvent (ethanol-precipitated synthesis). Briefly, 10.1 g $Ce(NO_3)_3{\cdot}6H_2O$ was dissolved rapidly in 60 mL ethanol solution, then 9 mL of 28 wt% ammonia solution diluted by 9 mL of ethanol was added into the $Ce(NO_3)_3{\cdot}6H_2O$ solution. After stirring of 2 h, the precipitate was filtered, washed with ethanol solution, and then dried at 60 °C overnight. Finally, the sample was calcined at 500 °C in air for 2 h.

CeO_2-w was prepared by precipitation method using water as solvent (water-precipitated synthesis). 10.1 g $Ce(NO_3)_3{\cdot}6H_2O$ was dissolved in 60 mL of distilled water, then 9 mL of 28 wt% ammonia solution diluted by 9 mL of distilled water was added into the $Ce(NO_3)_3{\cdot}6H_2O$ solution, then the solution was stirred for 2 h at 50 °C. The following preparation steps were as same as those of CeO_2-e.

The as-obtained CeO_2 was impregnated by ruthenium (III) nitrosyl nitrate solution (Aldrich) and the theoretical ratio of Ru to CeO_2 was fixed to 3 wt%.

2.2. Catalyst evaluation and characterization

The ammonia synthesis evaluations were performed in a fixed bed stainless steel reactor. Before ammonia synthesis, 0.3 g of catalysts mixed with quartz sand (1:20 vol./vol.) and then activated at 500 °C in the 75 %H_2–25 %N_2 mixed gas for 5 h. The ammonia synthesis rates were obtained at 400 °C, 1 MPa and 36000 mL g_{cat}^{-1} h^{-1}. During activity test, H_2SO_4 solution was used to trap ammonia in the outlet gas, and the concentration of NH_4^+ was analyzed by ICS-600 analysis. The ammonia synthesis rates were calculated by the following equation:

$$\text{reaction rate} = \frac{\text{mol of} NH_4^+}{\text{mass of catalyst(g)} \times \text{time(h)}} \quad (1)$$

The color change reaction of the mixtures of catalysts and WO_3 was operated on a Micromeritics AutoChem II 2920. The mass ratio of catalysts and WO_3 in the mixture is 1:30. The mixture was placed in a quartz reaction tube. The hydrogen was then flowed through the reaction tube at a rate of 50 mL min^{-1}. Any color changes of the powder samples with the time were observed in the process. Photographs of mixture before treatment (0 s) and after treatment with H_2 at 100 °C for 1 min, 3 min and 30 min were collected.

Other characterization details including X-ray photoelectron spectroscopy (XPS), hydrogen temperature-programmed reduction (H_2-TPR), X-ray diffraction (XRD), N_2 physisorption, transmission electron microscopy (TEM), Raman, Diffuse reflectance infrared Fourier transform spectroscopy (DRIFTS) and H_2/D_2 exchange experiment are provided in supplementary information.

3. Results and discussion

3.1. Evaluation of the catalytic performance

Fig. 1 shows that the ammonia synthesis rates of Ru catalysts decrease with decreasing temperatures (350–400 °C), and the activation energies are 51.5 and 58.3 kJ mol^{-1} for Ru/CeO_2-w and Ru/CeO_2-e, respectively, suggesting that Ru/CeO_2-w and Ru/CeO_2-e have a similar reaction mechanism of ammonia synthesis. Two catalysts both exhibit excellent stable performance in ammonia production, and no significant deactivation is found for more than 100 h. As summarized in Table S1, Ru/CeO_2-w shows the impressive catalytic activity, and the estimated turnover frequencies (TOF) at different space velocities (18,000–72,000 mL g^{-1} h^{-1}) are all superior to the oxide-supported Ru catalysts reported in the literature [11,14,25–31]. The ammonia production rate of Ru/CeO_2-w is 22.6 mmol g_{cat}^{-1} h^{-1} at 1.0 MPa and 400 °C, while the catalytic activity of Ru/CeO_2-e is only 4.6 mmol g_{cat}^{-1} h^{-1}. This result indicates that the difference in the solvent for the preparation of ceria strongly affects the ammonia synthesis activity of Ru/CeO_2 catalysts. As it can be seen from Table S2, the NH_3 reaction orders of Ru/CeO_2-w and Ru/CeO_2-e are − 0.75 and − 0.66, respectively, and the N_2 reaction orders are 0.96 and 0.80 for Ru/CeO_2-w and Ru/CeO_2-e, respectively. These results indicate that the significant difference in catalytic activity could not be attributed to the change in N_2 activation or NH_3 desorption. On the other hand, the H_2 reaction orders are 1.01 and 0.43 for Ru/CeO_2-w and Ru/CeO_2-e, respectively. The enhancement of H_2 reaction order indicates that hydrogen poisoning phenomenon is suppressed for Ru/CeO_2-w, consistent with the observation of Lin et al. [32]. In such a case, when the reaction pressure is increased from 1 to 10 MPa, the ammonia synthesis activities increase by more than 82.1 % and 64.5 % for Ru/CeO_2-w and Ru/CeO_2-e, respectively. That is, the catalytic activities of Ru/CeO_2-w increase more significantly than those of Ru/CeO_2-e with increasing of the reaction pressures, revealing that Ru/CeO_2-w shows an excellent high-pressure effect because of the weaker hydrogen poisoning effect [13,29,33–35].

3.2. Structural characterizations of the catalysts

SEM images show that the sizes of CeO_2 particles for CeO_2-w and CeO_2-e are 12.8 and 11.1 nm (Fig. S1), respectively, indicating that the presence of water during the ceria preparation leads to a slight enhancement of grain size of ceria, which is in line with previous work

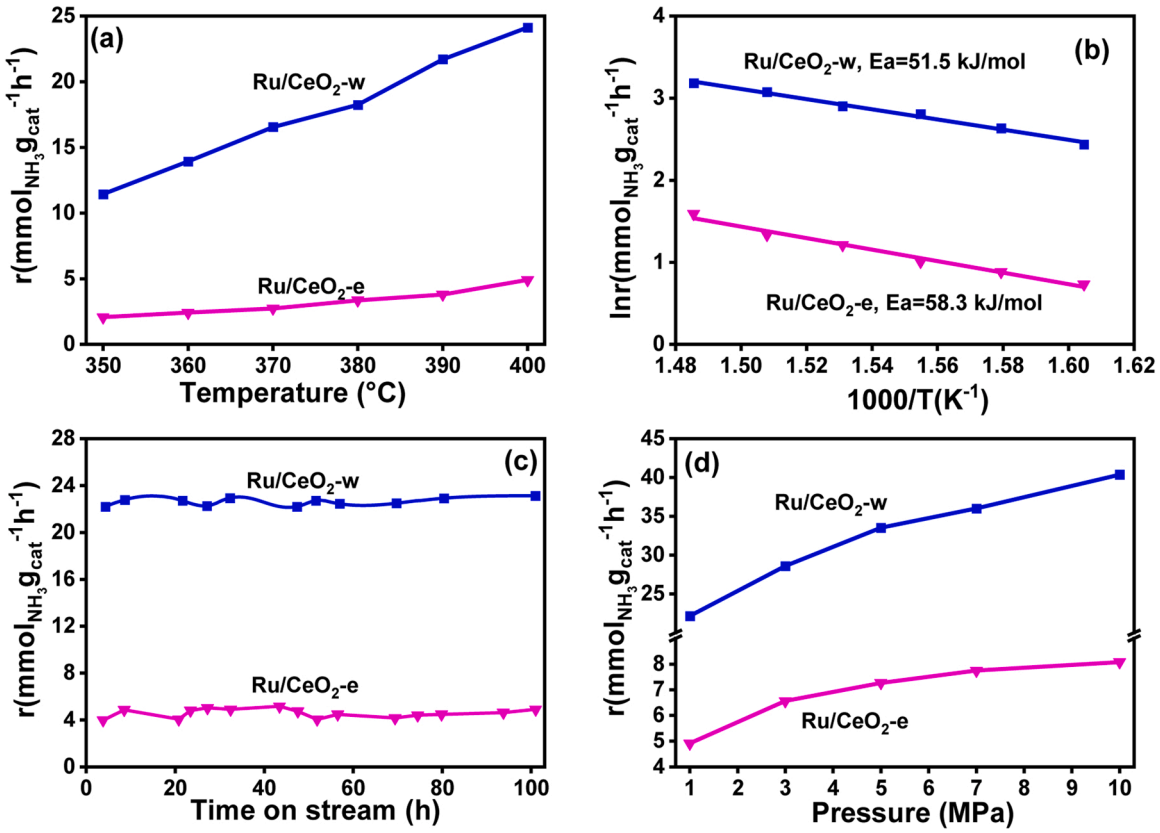

Fig. 1. (a) Correlation of NH_3 synthesis rates with temperature, (b) Arrhenius plots of NH_3 synthesis rates over Ru catalysts, (c) Correlation of NH_3 synthesis rates with time at 400 °C and 1.0 MPa and (d) Correlation of NH_3 synthesis rates with pressure at 400 °C, 3:1 of H_2/N_2 ratio and 36,000 mL g^{-1} h^{-1}.

[36]. The surface areas of Ru/CeO_2-w and Ru/CeO_2-e are 38 and 49 m^2 g^{-1} (Table S3), respectively. The results indicate that the notable variation in the catalytic activity between Ru/CeO_2-w and Ru/CeO_2-e cannot be simply attributed to the slight difference in grain size or surface area between Ru/CeO_2-w and Ru/CeO_2-e. As shown in Fig S2, only typical cubic fluoride crystal phase of CeO_2 can be detected in the XRD patterns of CeO_2 supports and Ru catalysts. There is a lack of diffraction peaks for Ru species (at about 44°) or Ru oxide (at around 28° or 35°) in Fig. S2, suggesting that the Ru species are uniformly distributed on the CeO_2 surface. As shown in the HRTEM images of the fresh Ru/CeO_2 catalysts (Fig. S3), Ru particles with the sizes range of 0.5–1.0 nm are dispersed on the surface of CeO_2 for Ru/CeO_2-w and Ru/CeO_2-e, and the EDS mapping also confirms that the Ru species are highly dispersed (Fig. S4). Moreover, no significant increase in the size of Ru particles can be observed in the HRTEM images of the catalysts after the reaction (Fig. S5), indicating that Ru species would not agglomerate during the reaction, and the catalysts have good stability.

Raman spectra of CeO_2 show that there are four bands at 1180, 600, 465 and 260 cm^{-1} (Fig. S6), which are assignable to the second-order longitudinal optical vibration, defect-induced vibration related to oxygen vacancy associated with Ce^{3+}, symmetrical F_{2g} vibration of CeO_2 and second-order transverse vibration, respectively [12,37–42]. $I_{(600+1180)}/I_{465}$ ratio, i.e. the number of oxygen vacancies and other defects [37,38,41], are 0.029 and 0.035 for CeO_2-w and CeO_2-e, respectively. XPS spectra of CeO_2 also show that the Ce^{3+} concentrations are 25.5 % and 32.3 % for CeO_2-w and CeO_2-e, respectively (Fig. S7), which is consistent with the Raman observation, confirming that there are a larger number of defects for CeO_2-e. Moreover, there are two peaks at 529.4 (O_α) and 531.3 eV (O_β) in the O 1 s spectra of Ru catalysts, which originate from lattice oxygen and oxide defects or surface oxygen ions, respectively [38,41]. CeO_2-e has a higher ratio of O_β/O_α, indicating that there is a larger amount of surface oxygen in the ceria obtained by ethanol-precipitated synthesis.

It has been found that the addition of Ru species into CeO_2 could activate lattice oxygen to creation oxygen vacancy [43,44]. As a result, the introduction of Ru species leads to a slight increase of $I_{(600+1180)}/I_{465}$ ratio (Fig. 2), but the difference in the $I_{(600+1180)}/I_{465}$ ratio is slight because of the similar Ru loading between Ru/CeO_2-w and Ru/CeO_2-e. The result reveals that the change in the solvent of cerium nitrate during the preparation of ceria slightly affects the number of oxygen vacancies or other defects for Ru catalysts studied in present work. On the other hand, the introduction of Ru species results in the shift of the Raman peaks of second-order transverse vibration and F_{2g} vibration mode to lower wavenumber (240 and 452 cm^{-1}), implying that there is an electronic interaction between Ru and ceria for Ru catalysts [45,46]. Moreover, there are two clear bands at 695 and 967 cm^{-1} in Raman spectra of Ru catalysts. These bands could be attributed to Ru−O−Ce structure [41], and the peak intensity ratio of Ru−O−Ce structure and the $F_{2\,g}$ mode ($I_{695+967}/I_{452}$) represents the concentration of Ru−O−Ce interfacial bond [41,42,47]. The $I_{695+967}/I_{452}$ ratios are 0.07 and 0.23 for Ru/CeO_2-w and Ru/CeO_2-e, respectively, indicating that Ru/CeO_2-w has the lower Ru−O−Ce concentration compared with Ru/CeO_2-e.

For the reducible metal oxides-supported metal catalysts with strong metal-support interaction (SMSI), some metal species would be capsulated by suboxide overlayers [48–54]. As confirmed by XPS results (Fig. 2), the I_{Ru3d}/I_{Ce3d} ratio of Ru/CeO_2-w is 0.035, which is higher than that of Ru/CeO_2-e (0.013). This result suggests that more Ru species would be covered by suboxide overlayers for Ru/CeO_2-e, and the change in intensity percentage of Ce^{3+} peaks to total Ce XPS peaks between Ru/CeO_2-w and Ru/CeO_2-e also confirms that Ru/CeO_2-e has a larger amount of Ce^{3+} species. There are metallic Ru (Ru^0) and Ru oxides ($Ru^{\delta+}$) in Ru catalysts (Fig. 2), the $Ru^0/(Ru^0+Ru^{n+})$ value of Ru/CeO_2-e (0.37) is lower than that of Ru/CeO_2-w (0.73). This result indicates that Ru/CeO_2-e has a larger amount of the oxidized Ru species, which would

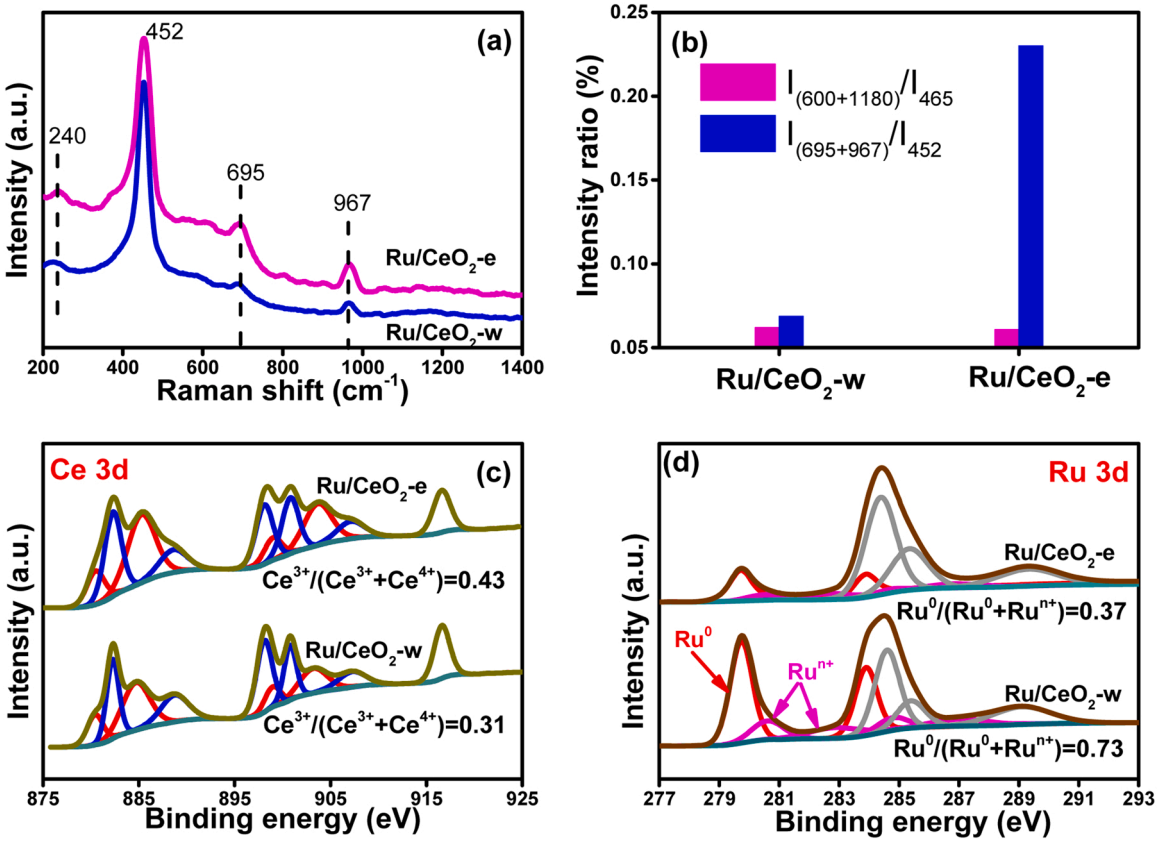

Fig. 2. (a) Raman spectra for various Ru catalysts, (b) $I_{695+967}/I_{456}$ and $I_{600+1180}/I_{465}$ intensity ratios of Ru catalysts, XPS spectra of Ru catalysts (c) Ce 3d and (d) Ru 3d.

mainly locate at the Ru-oxide interfaces [55]. On the other hand, there is no significant difference in the Ru binding energy between Ru/CeO_2-e and Ru/CeO_2-w, revealing that the change in Ru electronic property does not play a crucial role in improving the ammonia synthesis rates for Ru/CeO_2-w in comparison to Ru/CeO_2-e. As shown in Fig. S8, there are two peaks at 529.4 (O_α) and 531.4 eV (O_β) in the O 1 s spectrum of Ru/CeO_2-w, which can be attributed to the lattice oxygen and active oxygen species [41,56–58]. Moreover, the area ratios of O_α and O_β peaks to the total oxygen peaks in Ru/CeO_2-w are 0.78 and 0.22, respectively. In contrast, besides O_α and O_β peaks, a new O 1 s peak (O_γ), which can be related to oxygen species in cerium suboxide (Ce_2O_3) [57,58], appears at 530.3 eV in the O 1 s spectrum of Ru/CeO_2-e. The area ratios of O_α, O_γ and O_β peaks to the total oxygen peaks in Ru/CeO_2-e are 0.48, 0.34 and 0.18, respectively. These results confirm that there are multiple oxygen species including lattice oxygen in ceria and surface active oxygen over Ru/CeO_2 catalysts (Ru/CeO_2-e and Ru/CeO_2-w), moreover, there are a larger amount of oxygen species in cerium suboxide for Ru/CeO_2-e.

As shown in Fig. 3a, the Ru surface sites were further studied by CO diffuse-reflectance infrared Fourier transform spectroscopy (DRIFTS), and Fig. 3b displays the possible adsorption configurations. The DRIFTS spectra of Ru catalysts both have a peak at 2170 cm^{-1}, which is assigned to CO in the gas phase [59]. In the meantime, other three IR bands could

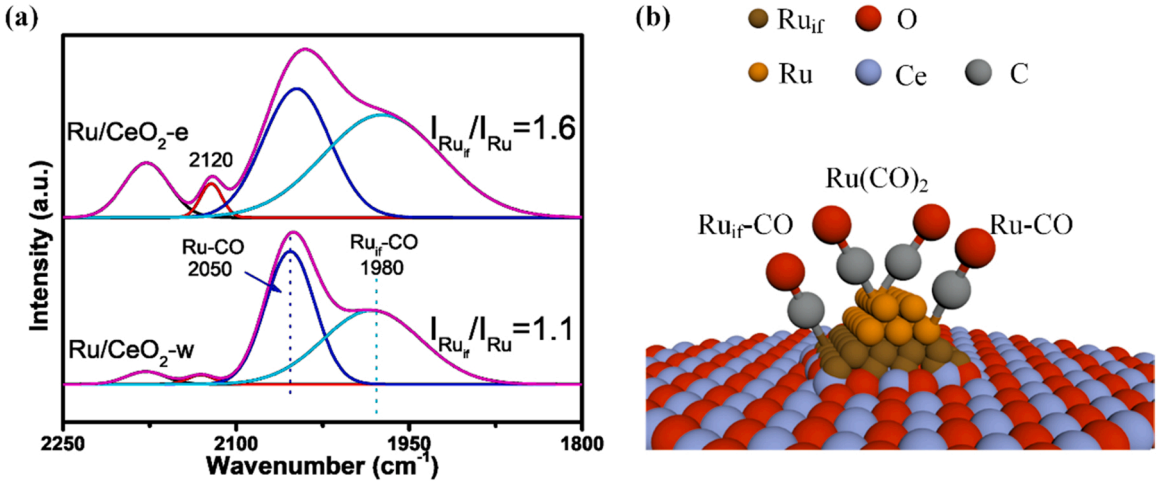

Fig. 3. (a) CO-DRIFTS of Ru/CeO_2 catalysts and (b) CO adsorption configurations on Ru/CeO_2-e catalysts.

be detected at 1980, 2050 and 2120 cm^{-1}, which could be attributed to the adsorbed CO adsorbed on Ru-CeO_2 interface sites (Ru_{if}−CO), CO species on the Ru top sites (Ru−CO) and multicarbonyl species adsorbed on Ru sites with low coordination numbers ($Ru(CO)_x$, $x = 2$, 3), respectively [20,55,60]. The proportion of 1980 cm^{-1} band correlated with Ru_{if}−CO for Ru/CeO_2-e is higher than that for Ru/CeO_2-w, confirming that a large number of Ru species is located at Ru-ceria interfaces for Ru/CeO_2-e, agreeing with the Raman and XPS results.

3.3. Hydrogen migration and adsorption property of Ru catalysts

As displayed in Fig. 4a, in the H_2-TPR profile of as-prepared Ru/CeO_2-w, there is only a sharp hydrogen consumption peak between 100 °C and 180 °C, and the maximum temperature is about 135 °C. On the contrary, there is another hydrogen consumption peak centered at 198 °C in addition to the peak of 100–180 °C during hydrogen treatment of the as-prepared Ru/CeO_2-e. The low hydrogen reduction peak can be assigned to the reduction of Ru oxide weakly reacted with CeO_2, and the second peak at 198 °C can be correlated with Ru species strongly reacted with CeO_2 or incorporated into CeO_2 surface [22,23,41]. The total hydrogen consumptions are similar between the as-prepared Ru/CeO_2-w and Ru/CeO_2-e (Table S4), however, these data are lower than the theoretical values for the reduction of Ru species, indicating that some Ru species would not be reduced to metallic Ru. Moreover, there is a great deal of hydrogen consumption for Ru/CeO_2-w during H_2-TPR study of Ru catalysts oxidized in oxygen at 150 °C, indicating that a higher ratio of Ru species can be oxidized for Ru/CeO_2-w due to the weaker Ru-CeO_2 interaction, which is consistent with the observation of Raman and XPS measurements.

It can be imaged that the difference in the proportion interfacial Ru species, the concentration of Ru−O−Ce and the ratio of metallic Ru would strongly affect the hydrogen migration/spillover and the adsorption property of reaction gases. It has been found that blue H_xWO_3 would form during hydrogen reduction of yellow WO_3 [17,61], thus a color change experiment over the mixture of WO_3 and Ru catalysts is designed to investigate the mobility of hydrogen species. As depicted in Fig. 5, hydrogen treatment of the mixture of WO_3 and Ru/CeO_2-w at 100 °C leads to the color change from light yellow to dark blue in 30 min, conversely, no distinct color change is observed for the mixture of Ru/CeO_2-e and WO_3. These results reveal that the migration of hydrogen atoms on Ru particles to neighboring WO_3 on Ru/CeO_2-w is easier than that on Ru/CeO_2-e.

The quick hydrogen migration would contribute to the exchange of hydrogen species on Ru catalysts. As shown in Fig. 6, the mass signals of $m/z = 2$, 3 and 4 appear more quickly for Ru/CeO_2-w than that for Ru/CeO_2-e when a 50 % D_2 in H_2 mixture is introduced, and these mass signals disappear more quickly for Ru/CeO_2-w when the D_2 and H_2 mixture is switched over to Ar stream. In the meantime, Ru/CeO_2-w also shows higher intensity of $m/z = 3$ signal. Moreover, a larger amount of NH_x ($m/z = 15$ or 16) would release from Ru/CeO_2-w during TPSR measurement (Fig. S9). These results clearly suggest that the activation and the exchange of hydrogen species would be boosted over Ru/CeO_2-w in comparison to Ru/CeO_2-e.

The TPD experiments are used to further explore the adsorption/desorption properties of reactants. There are three hydrogen desorption peaks located at 115, 260 and 425 °C on Ru/CeO_2-e (Fig. 7). The former two peaks could be attributed to the desorption of the weak adsorbed hydrogen species (or subsurface RuH_x) and the strong adsorbed hydrogen species on Ru sites, while the last peak is assigned to the spillover hydrogen species from ceria [62,63]. Conversely, there are a larger amount of hydrogen species, which are related to Ru species, would desorb from Ru/CeO_2-w. Moreover, the intensity of the high-temperature hydrogen desorption decreases significantly for Ru/CeO_2-w. On the other hand, no N_2 desorption can be detected for Ru/CeO_2-e, while a weak and broad N_2 desorption peak could be observed for Ru/CeO_2-w. These results indicate that Ru/CeO_2-w shows excellent adsorption capacity for hydrogen and nitrogen species, which might be due to the higher proportion of metallic Ru in Ru/CeO_2-w.

3.4. Effect of hydrogen migration on ammonia synthesis performances

As mentioned above, two cerium oxides, which are prepared by ethanol-precipitated synthesis (CeO_2-e) and water-precipitated synthesis (CeO_2-w), both show typical cubic fluoride crystal phase of CeO_2. However, the sample obtained by ethanol-precipitated synthesis has multiple oxygen species and a larger amount of Ce^{3+} concentration and defects. The change in the properties of ceria would strongly affect the Ru−CeO_2 interactions for Ru/CeO_2 catalysts. The MSI between Ru and ceria strongly affects the ammonia synthesis activity of Ru/CeO_2 catalysts [22,23,46,62,64]. However, metal−support interactions contain different forms, such as the SMSI, EMSI, the formation of interface sites and the change in chemical composition [54]. No distinct change in the Ru binding energy between Ru/CeO_2-e and Ru/CeO_2-w is observed (Fig. 2), implying that there is no difference in EMSI for Ru catalysts. However, the difference in the properties of ceria strongly affects the formation of Ru−O−Ce bond as well as the existing forms of Ru species and Ce species for Ru/CeO_2 catalyst. As shown in Fig. 8, a larger amount of Ru species covered by suboxide overlayers for the Ru catalyst supported on ceria obtained by ethanol-precipitated synthesis (Ru/CeO_2-e), leading to enhancement of Ce^{3+} concentration on the Ru surface or the Ru-CeO_2 interface. In the meantime, the presence of a larger amount of oxygen species on ceria would facilitate the contact and interaction between oxygen species and Ru species for CeO_2-e. As a result, there is a large amount of Ru−O−Ce interfacial sites in Ru/CeO_2-e, leading to lowering of the number of the Ru metal as well as exposed Ru species.

It is well known that the reaction of ammonia synthesis is composed

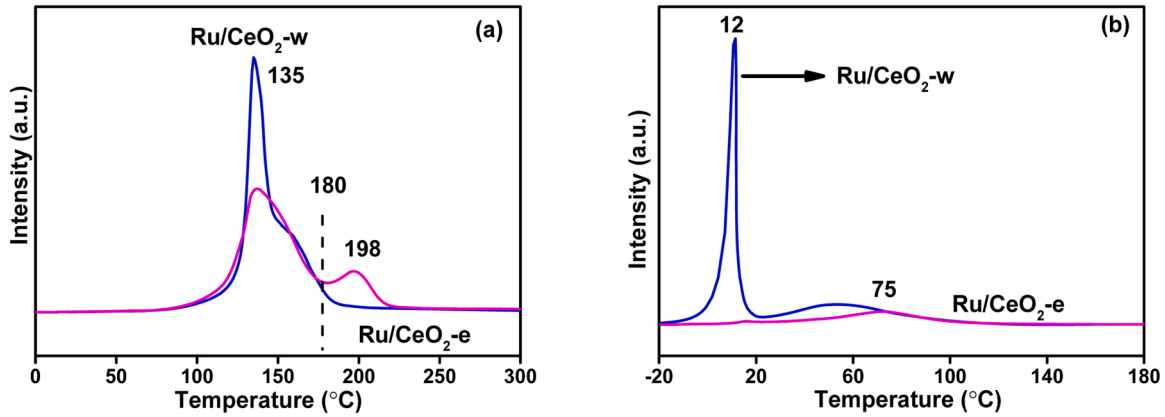

Fig. 4. (a) H_2-TPR profiles of the Ru catalysts without hydrogen reduction and (b) H_2-TPR profiles of the samples oxidized in oxygen at 150 °C.

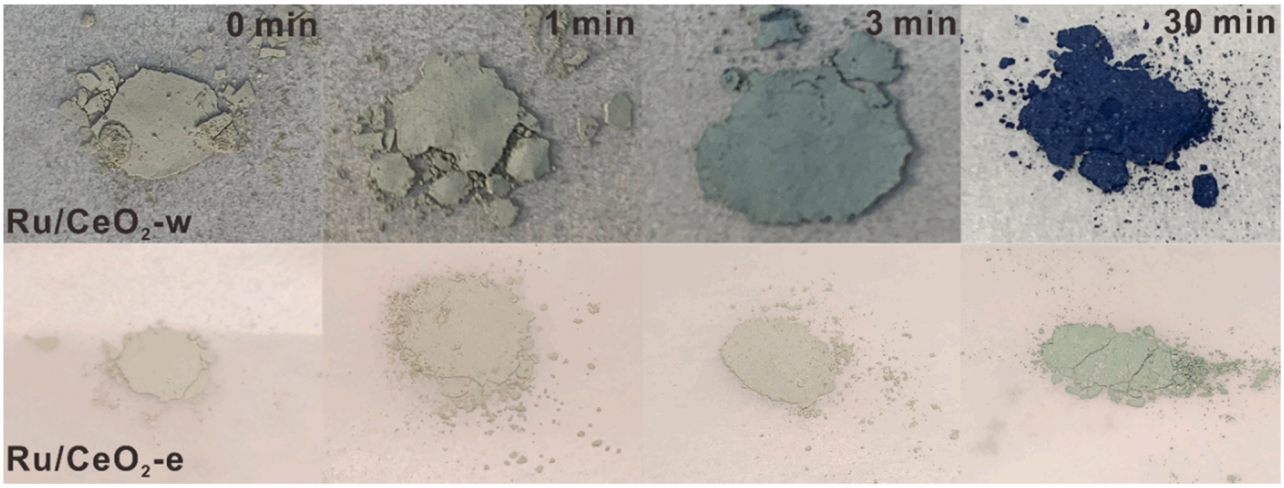

Fig. 5. Photographs of the mixture of WO_3 and Ru catalysts before treatment (0 s) and after hydrogen treatment at 100 °C for various time.

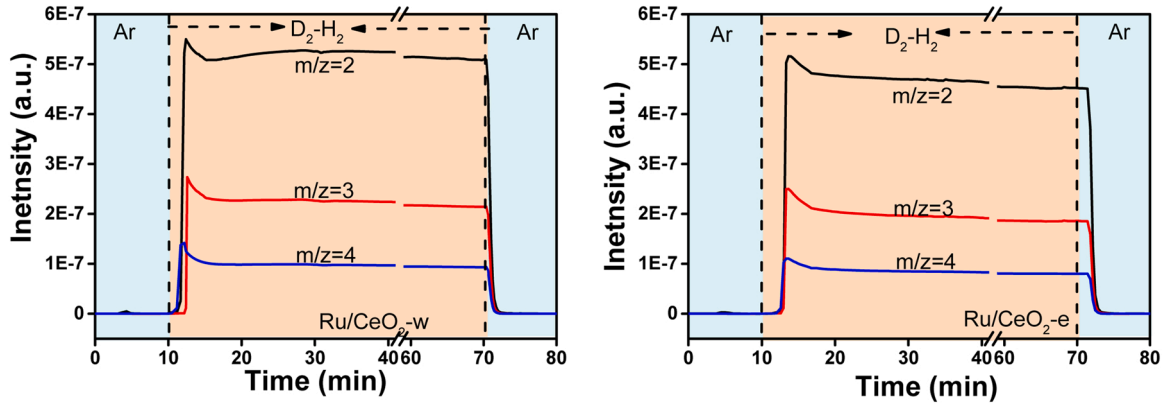

Fig. 6. H_2/D_2 exchange experiment over Ru catalysts at 400 °C (Left) Ru/CeO_2-w and (Right) Ru/CeO_2-e.

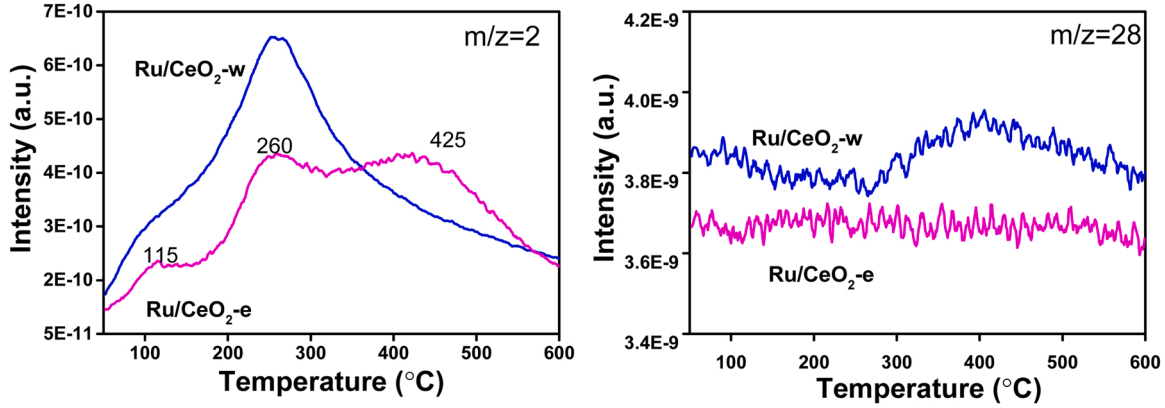

Fig. 7. Mass signals of H_2 and N_2 during the N_2-H_2-TPD experiments of Ru catalysts.

of various reaction steps [65,66], including the activation of nitrogen and hydrogen species, the reaction of nitrogen and hydrogen to form NH_x intermediate species, and the desorption of ammonia or other unreacted reactants. Among these steps, N_2 dissociation is usually argued as the rate-determining step for the conventional Fe or Ru catalysts because of the high nitrogen triple bond energy, and the N_2 reaction order is in the range of 0.8–1.0 [67,68]. Herein the N_2 reaction orders are 0.96 and 0.80 for Ru/CeO_2-w and Ru/CeO_2-e, respectively, indicating that the significant difference in ammonia synthesis activity could not be attributed to the improvement in N_2 activation. On the other hand, the activation of N_2 and that of H_2 are competitive steps because these steps both are preferentially occurred on the Ru sites [69]. In the case of Ru/CeO_2-e, the amount of Ru species covered by CeO_2 overlayers would enhance, and the number of Ru−O−Ce interfacial sites also increase. As a result, hydrogen spillover from Ru species to ceria would be boosted, and thus the high-temperature hydrogen desorption peak could be found during the TPD experiment of Ru/CeO_2-e pre-absorbed the N_2 and H_2 mixed gas (Fig. 7). The enrichment of the strong

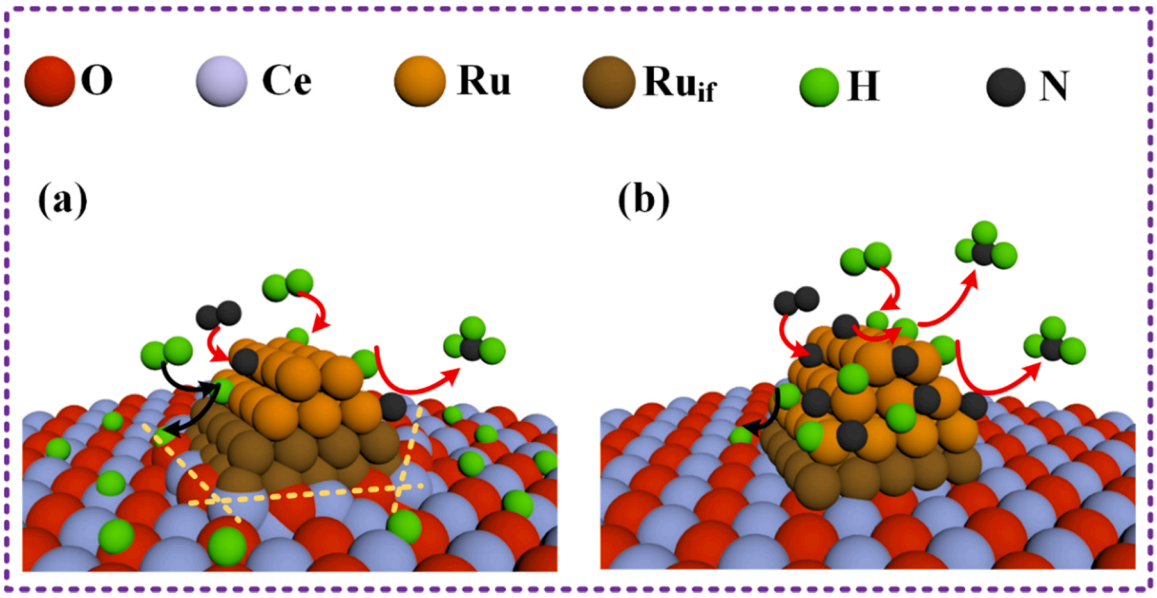

Fig. 8. Schematic illustration of Ru catalysts (a) Ru/CeO_2-e and (b) Ru/CeO_2-w.

adsorbed hydrogen species could inhibit the subsequent process of ammonia synthesis, moreover, the decrease in the amount of the exposed Ru species and the proportion of Ru metal would result in the lowering of Ru sites available for hydrogen activation and migration. As a result, the color change of the mixture of WO_3 and Ru/CeO_2-e is less significant than that of the mixing WO_3 and Ru/CeO_2-w (Fig. 5). The formation of HD is also slower for Ru/CeO_2-e during H_2/D_2 exchange experiment (Fig. 6). Whereas in the case of Ru/CeO_2-w, the weaker MSI leads to the increase of the proportion of metallic Ru as well as the amount of the exposed Ru species. A larger number of Ru species could participate in the reaction of NH_3 synthesis, and the inhibition of the strong hydrogen adsorption is weaker. In such a case, the migration and desorption of hydrogen species would be accelerated, and then the nitrogen desorption peak could be found in the TPD profiles of Ru catalysts supported on ceria obtained by water-precipitated synthesis (Fig. 7). As a result, Ru/CeO_2-w show higher reaction order with respect to H_2 than Ru/CeO_2-e because the hydrogen poisoning would be alleviated for Ru/CeO_2-w. In such a case, Ru/CeO_2-w shows 4.9-fold higher in ammonia synthesis activity than the sample with ceria prepared by the ethanol-precipitated synthesis, and Ru/CeO_2-w also shows an excellent high-pressure effect in ammonia synthesis.

4. Conclusions

The difference in the properties of ceria could strongly affect the Ru−CeO_2 interactions for ceria-supported Ru catalysts. Compared to Ru catalyst supported on ceria obtained by water-precipitated synthesis (Ru/CeO_2-w), the sample with ceria prepared by the ethanol-precipitated synthesis (Ru/CeO_2-e) has more kinds of oxygen species and larger number of Ru−O−Ce interfacial sites, defects and Ce^{3+} concentration, causing the SMSI between Ru and ceria. In such a case, the quantity of the exposed Ru species and the ratio of Ru metal are lower, moreover, the number of the strong adsorbed hydrogen species is larger. As a result, the migration and desorption of hydrogen species are slowed down, and then the N_2 dissociation, H_2 activation and the reaction of ammonia synthesis would be inhibited. Therefore, Ru/CeO_2-w has 4.9-fold higher in catalytic activity than Ru/CeO_2-e, and also shows an excellent high-pressure effect in ammonia synthesis. This work demonstrates that the enhancement of hydrogen migration leads to enhancement of the ammonia synthesis activity for ceria-supported Ru catalysts, which can be extended to other heterogeneous hydrogen-involved catalytic reactions.

CRediT authorship contribution statement

Chunyan Li:·Investigation, Writing – original draft, Visualization. **Minghui Li:** Conceptualization, Investigation. **Yiping Zheng:** Investigation. **Biyun Fang:** Investigation. **Jianxin Lin:** Investigation. **Jun·Ni:** Investigation. **Bingyu Lin:** Supervision, Investigation, Writing – review & editing, Visualization, Funding acquisition. **Lilong Jiang:** Supervision, Writing – review & editing, Funding acquisition.

Declaration of Competing Interest

The authors declare that they have no known competing financial interests or personal relationships that could have appeared to influence the work reported in this paper.

Data availability

Data will be made available on request.

Acknowledgements

This work was supported by the National Natural Science Foundation of China (Grants 22038002 and 22178061) and Natural Science Foundation for Distinguished Young Scholars of Fujian Province (2022J06012).

Appendix A. Supporting information

Supplementary data associated with this article can be found in the online version at doi:10.1016/j.apcatb.2022.121982.

References

[1] L. Wang, M. Xia, H. Wang, K. Huang, C. Qian, C.T. Maravelias, G.A. Ozin, Greening ammonia toward the solar ammonia refinery, Joule 2 (2018) 1055–1074.
[2] J.W. Erisman, M.A. Sutton, J. Galloway, Z. Klimont, W. Winiwarter, How a century of ammonia synthesis changed the world, Nat. Geosci. 1 (2008) 636–639.
[3] N.V. Rees, R.G. Compton, Carbon-free energy: a review of ammonia- and hydrazine-based electrochemical fuel cells, Energy Environ. Sci. 4 (2011) 1255–1260.

[4] A. Klerke, C.H. Christensen, J.K. Nørskov, T. Vegge, Ammonia for hydrogen storage: challenges and opportunities, J. Mater. Chem. 18 (2008) 2304–2310.
[5] A. Wu, J. Yang, B. Xu, X.-Y. Wu, Y. Wang, X. Lv, Y. Ma, A. Xu, J. Zheng, Q. Tan, Y. Peng, Z. Qi, H. Qi, J. Li, Y. Wang, J. Harding, X. Tu, A. Wang, J. Yan, X. Li, Direct ammonia synthesis from the air via gliding arc plasma integrated with single atom electrocatalysis, Appl. Catal. B Environ. 299 (2021), 120667.
[6] J. Humphreys, R. Lan, S. Chen, M. Walker, Y. Han, S. Tao, Cation doped cerium oxynitride with anion vacancies for Fe-based catalyst with improved activity and oxygenate tolerance for efficient synthesis of ammonia, Appl. Catal. B 285 (2021), 119843.
[7] D.R. MacFarlane, P.V. Cherepanov, J. Choi, B.H.R. Suryanto, R.Y. Hodgetts, J. M. Bakker, F.M. Ferrero Vallana, A.N. Simonov, A roadmap to the ammonia economy, Joule 4 (2020) 1186–1205.
[8] G. Zhang, Y. Meng, B. Xie, Z. Ni, H. Lu, S. Xia, Precise location and regulation of active sites for highly efficient photocatalytic synthesis of ammonia by facet-dependent $BiVO_4$ single crystals, Appl. Catal. B Environ. 296 (2021), 120379.
[9] D.E. Brown, T. Edmonds, R.W. Joyner, J.J. McCarroll, S.R. Tennison, The genesis and development of the commercial BP doubly promoted catalyst for ammonia synthesis, Catal. Lett. 144 (2014) 545–552.
[10] Y. Izumi, Y. Iwata, K.-i Aika, Catalysis on ruthenium clusters supported on CeO_2 or Ni-doped CeO_2: adsorption behavior of H_2 and ammonia synthesis, J. Phys. Chem. 100 (1996) 9421–9428.
[11] Z. Ma, S. Zhao, X. Pei, X. Xiong, B. Hu, New insights into the support morphology–dependent ammonia synthesis activity of Ru/CeO_2 catalysts, Catal. Sci. Technol. 7 (2017) 191–199.
[12] B. Lin, Y. Liu, L. Heng, X. Wang, J. Ni, J. Lin, L. Jiang, Morphology effect of ceria on the catalytic performances of Ru/CeO_2 catalysts for ammonia synthesis, Ind. Eng. Chem. Res. 57 (2018) 9127–9135.
[13] Y. Wu, C. Li, B. Fang, X. Wang, J. Ni, B. Lin, J. Lin, L. Jiang, Enhanced ammonia synthesis performance of ceria-supported Ru catalysts via introduction of titanium, Chem. Commun. 56 (2020) 1141–1144.
[14] C. Li, Z. Zhang, Y. Zheng, B. Fang, J. Ni, J. Lin, B. Lin, X. Wang, L. Jiang, Titanium modified Ru/CeO_2 catalysts for ammonia synthesis, Chem. Eng. Sci. 251 (2022), 117434.
[15] Z. Li, K. Werner, K. Qian, R. You, A. Płucienik, A. Jia, L. Wu, L. Zhang, H. Pan, H. Kuhlenbeck, S. Shaikhutdinov, W. Huang, H.-J. Freund, Oxidation of reduced ceria by incorporation of hydrogen, Angew. Chem. Int. Ed. 58 (2019) 14686–14693.
[16] R.T. Yang, Y. Wang, Catalyzed hydrogen spillover for hydrogen storage, J. Am. Chem. Soc. 131 (2009) 4224–4226.
[17] M. Xiong, Z. Gao, P. Zhao, G. Wang, W. Yan, S. Xing, P. Wang, J. Ma, Z. Jiang, X. Liu, J. Ma, J. Xu, Y. Qin, In situ tuning of electronic structure of catalysts using controllable hydrogen spillover for enhanced selectivity, Nat. Commun. 11 (2020) 4773.
[18] Y. Li, R.T. Yang, Hydrogen storage in metal−organic frameworks by bridged hydrogen spillover, J. Am. Chem. Soc. 128 (2006) 8136–8137.
[19] W. Karim, C. Spreafico, A. Kleibert, J. Gobrecht, J. VandeVondele, Y. Ekinci, J. A. van Bokhoven, Catalyst support effects on hydrogen spillover, Nature 541 (2017) 68–71.
[20] X. Li, J. Lin, L. Li, Y. Huang, X. Pan, S.E. Collins, Y. Ren, Y. Su, L. Kang, X. Liu, Y. Zhou, H. Wang, A. Wang, B. Qiao, X. Wang, T. Zhang, Controlling CO_2 hydrogenation selectivity by metal-supported electron transfer, Angew. Chem. Int. Ed. 59 (2020) 19983–19989.
[21] F. Yang, X. Bao, P. Li, X. Wang, G. Cheng, S. Chen, W. Luo, Boosting hydrogen oxidation activity of Ni in alkaline media through oxygen-vacancy-rich CeO_2/Ni heterostructures, Angew. Chem. Int. Ed. 58 (2019) 14179–14183.
[22] C. Li, F. Liu, Y. Shi, Y. Zheng, B. Fang, J. Lin, J. Ni, X. Wang, B. Lin, L. Jiang, Inducing the metal–support interaction and enhancing the ammonia synthesis activity of ceria-supported ruthenium catalyst via N_2H_4 reduction, ACS Sustain. Chem. Eng. 9 (2021) 4885–4893.
[23] C. Li, Y. Shi, Z. Zhang, J. Ni, X. Wang, J. Lin, B. Lin, L. Jiang, Improving the ammonia synthesis activity of Ru/CeO_2 through enhancement of the metal–support interaction, J. Energy Chem. 60 (2021) 403–409.
[24] C. Mao, J. Wang, Y. Zou, G. Qi, J.Y. Yang Loh, T. Zhang, M. Xia, J. Xu, F. Deng, M. Ghoussoub, N.P. Kherani, L. Wang, H. Shang, M. Li, J. Li, X. Liu, Z. Ai, G. A. Ozin, J. Zhao, L. Zhang, Hydrogen spillover to oxygen vacancy of $TiO_{2-x}H_y$/Fe: breaking the scaling relationship of ammonia synthesis, J. Am. Chem. Soc. 142 (2020) 17403–17412.
[25] M. Kitano, Y. Inoue, M. Sasase, K. Kishida, Y. Kobayashi, K. Nishiyama, T. Tada, S. Kawamura, T. Yokoyama, M. Hara, H. Hosono, Self–organized ruthenium–barium core–shell nanoparticles on a mesoporous calcium amide matrix for efficient low–temperature ammonia synthesis, Angew. Chem. Int. Ed. 57 (2018) 2648–2652.
[26] K. Sato, K. Imamura, Y. Kawano, S.-i Miyahara, T. Yamamoto, S. Matsumura, K. Nagaoka, A low–crystalline ruthenium nano–layer supported on praseodymium oxide as an active catalyst for ammonia synthesis, Chem. Sci. 8 (2017) 674–679.
[27] Y. Kobayashi, Y. Tang, T. Kageyama, H. Yamashita, N. Masuda, S. Hosokawa, H. Kageyama, Titanium–based hydrides as heterogeneous catalysts for ammonia synthesis, J. Am. Chem. Soc. 139 (2017) 18240–18246.
[28] Y. Lu, J. Li, T. Tada, Y. Toda, S. Ueda, T. Yokoyama, M. Kitano, H. Hosono, Water durable electride Y_5Si_3: electronic structure and catalytic activity for ammonia synthesis, J. Am. Chem. Soc. 138 (2016) 3970–3973.
[29] M. Kitano, Y. Inoue, Y. Yamazaki, F. Hayashi, S. Kanbara, S. Matsuishi, T. Yokoyama, S.-W. Kim, M. Hara, H. Hosono, Ammonia synthesis using a stable electride as an electron donor and reversible hydrogen store, Nat. Chem. 4 (2012) 934–940.
[30] Y. Ogura, K. Tsujimaru, K. Sato, S.-i Miyahara, T. Toriyama, T. Yamamoto, S. Matsumura, K. Nagaoka, Ru/$La_{0.5}Pr_{0.5}O_{1.75}$ catalyst for low–temperature ammonia synthesis, ACS Sustain. Chem. Eng. 6 (2018) 17258–17266.
[31] Y. Ogura, K. Sato, S.I. Miyahara, Y. Kawano, T. Toriyama, T. Yamamoto, S. Matsumura, S. Hosokawa, K. Nagaoka, Efficient ammonia synthesis over a Ru/$La_{0.5}Ce_{0.5}O_{1.75}$ catalyst pre–reduced at high temperature, Chem. Sci. 9 (2018) 2230–2237.
[32] B. Lin, Y. Wu, B. Fang, C. Li, J. Ni, X. Wang, J. Lin, L. Jiang, Ru surface density effect on ammonia synthesis activity and hydrogen poisoning of ceria-supported Ru catalysts, Chin. J. Catal. 42 (2021) 1712–1723.
[33] B. Lin, L. Heng, B. Fang, H. Yin, J. Ni, X. Wang, J. Lin, L. Jiang, Ammonia synthesis activity of alumina–supported ruthenium catalyst enhanced by alumina phase transformation, ACS Catal. 9 (2019) 1635–1644.
[34] T.N. Ye, S.W. Park, Y. Lu, J. Li, M. Sasase, M. Kitano, H. Hosono, Contribution of nitrogen vacancies to ammonia synthesis over metal nitride catalysts, J. Am. Chem. Soc. 142 (2020) 14374–14383.
[35] T.-N. Ye, S.-W. Park, Y. Lu, J. Li, M. Sasase, M. Kitano, T. Tada, H. Hosono, Vacancy-enabled N_2 activation for ammonia synthesis on an Ni-loaded catalyst, Nature 583 (2020) 391–395.
[36] Y.W. Zhang, R. Si, C.S. Liao, C.H. Yan, C.X. Xiao, Y. Kou, Facile alcohothermal synthesis, size–dependent ultraviolet absorption, and enhanced CO conversion activity of ceria nanocrystals, J. Phys. Chem. B 107 (2003) 10159–10167.
[37] H. Tan, J. Wang, S. Yu, K. Zhou, Support morphology–dependent catalytic activity of Pd/CeO_2 for formaldehyde oxidation, Environ. Sci. Technol. 49 (2015) 8675–8682.
[38] Z. Hu, X. Liu, D. Meng, Y. Guo, Y. Guo, G. Lu, Effect of ceria crystal plane on the physicochemical and catalytic properties of Pd/Ceria for CO and propane oxidation, ACS Catal. 6 (2016) 2265–2279.
[39] Z. Wu, M. Li, J. Howe, H.M. Meyer, S.H. Overbury, Probing defect sites on CeO_2 nanocrystals with well–defined surface planes by Raman spectroscopy and O_2 adsorption, Langmuir 26 (2010) 16595–16606.
[40] Z. Wu, M. Li, S.H. Overbury, On the structure dependence of CO oxidation over CeO_2 nanocrystals with well–defined surface planes, J. Catal. 285 (2012) 61–73.
[41] H. Huang, Q. Dai, X. Wang, Morphology effect of Ru/CeO_2 catalysts for the catalytic combustion of chlorobenzene, Appl. Catal. B Environ. 158–159 (2014) 96–105.
[42] Y. Guo, S. Mei, K. Yuan, D.-J. Wang, H.-C. Liu, C.-H. Yan, Y.-W. Zhang, Low–temperature CO_2 methanation over CeO_2–supported Ru single atoms, nanoclusters, and nanoparticles competitively tuned by strong metal–support interactions and H–spillover effect, ACS Catal. 8 (2018) 6203–6215.
[43] H.-T. Chen, First-principles study of CO adsorption and oxidation on Ru-doped CeO_2(111) surface, J. Phys. Chem. C 116 (2012) 6239–6246.
[44] H. Huang, Q. Dai, X. Wang, Morphology effect of Ru/CeO_2 catalysts for the catalytic combustion of chlorobenzene, Appl. Catal. B Environ. 158–159 (2014) 96–105.
[45] A.M. Rao, P.C. Eklund, S. Bandow, A. Thess, R.E. Smalley, Evidence for charge transfer in doped carbon nanotube bundles from Raman scattering, Nature 388 (1997) 257–259.
[46] B. Lin, B. Fang, Y. Wu, C. Li, J. Ni, X. Wang, J. Lin, C.-t Au, L. Jiang, Enhanced ammonia synthesis activity of ceria-supported ruthenium catalysts induced by CO activation, ACS Catal. 11 (2021) 1331–1339.
[47] F. Wang, C. Li, X. Zhang, M. Wei, D.G. Evans, X. Duan, Catalytic behavior of supported Ru nanoparticles on the {100}, {110}, and {111} facet of CeO_2, J. Catal. 329 (2015) 177–186.
[48] J. An, Y. Wang, J. Lu, J. Zhang, Z. Zhang, S. Xu, X. Liu, T. Zhang, M. Gocyla, M. Heggen, R.E. Dunin-Borkowski, P. Fornasiero, F. Wang, Acid–promoter–free ethylene methoxycarbonylation over ru–clusters/ceria: the catalysis of interfacial lewis acid–base pair, J. Am. Chem. Soc. 140 (2018) 4172–4181.
[49] Z. Zhang, Y. Wang, J. Lu, J. Zhang, M. Li, X. Liu, F. Wang, Pr-doped CeO_2 catalyst in the prins condensation–hydrolysis reaction: are all of the defect sites catalytically active? ACS Catal. 8 (2018) 2635–2644.
[50] J.C. Matsubu, S. Zhang, L. DeRita, N.S. Marinkovic, J.G. Chen, G.W. Graham, X. Pan, P. Christopher, Adsorbate–mediated strong metal–support interactions in oxide–supported Rh catalysts, Nat. Chem. 9 (2017) 120–127.
[51] H. Tang, Y. Su, B. Zhang, F. Lee Adam, A. Isaacs Mark, K. Wilson, L. Li, Y. Ren, J. Huang, M. Haruta, B. Qiao, X. Liu, C. Jin, D. Su, J. Wang, T. Zhang, Classical strong metal–support interactions between gold nanoparticles and titanium dioxide, Sci. Adv., 3, e1700231.
[52] J. Zhang, H. Wang, L. Wang, S. Ali, C. Wang, L. Wang, X. Meng, B. Li, D.S. Su, F.-S. Xiao, Wet–chemistry strong metal–support interactions in titania–supported Au catalysts, J. Am. Chem. Soc. 141 (2019) 2975–2983.
[53] A. Parastaev, V. Muravev, E. Huertas Osta, A.J.F. van Hoof, T.F. Kimpel, N. Kosinov, E.J.M. Hensen, Boosting CO_2 hydrogenation via size-dependent metal–support interactions in cobalt/ceria-based catalysts, Nat. Catal. 3 (2020) 526–533.
[54] T.W. van Deelen, C. Hernández Mejía, K.P. de Jong, Control of metal-support interactions in heterogeneous catalysts to enhance activity and selectivity, Nat. Catal. 2 (2019) 955–970.
[55] J. Zhou, Z. Gao, G. Xiang, T. Zhai, Z. Liu, W. Zhao, X. Liang, L. Wang, Interfacial compatibility critically controls Ru/TiO2 metal-support interaction modes in CO_2 hydrogenation, Nat. Commun. 13 (2022) 327.
[56] C. Li, F. Liu, Y. Shi, Y. Zheng, B. Fang, J. Lin, J. Ni, X. Wang, B. Lin, L. Jiang, Inducing the metal–support interaction and enhancing the ammonia synthesis activity of ceria–supported ruthenium catalyst via N_2H_4 reduction, ACS Sustain. Chem. Eng. 9 (2021) 4885–4893.

[57] J.R. Rumble, D.M. Bickham, C.J. Powell, The NIST x-ray photoelectron spectroscopy database, Surf. Interface Anal. 19 (2010) 241–246.
[58] C.D. Wagner, A.V. Naumkin, A. Kraut-Vass, J.W. Allison, J. Rumble, NIST standard reference database 20 version 4.1, (2003).
[59] W. Xu, R. Si, S.D. Senanayake, J. Llorca, H. Idriss, D. Stacchiola, J.C. Hanson, J. A. Rodriguez, In situ studies of CeO_2–supported Pt, Ru, and Pt–Ru alloy catalysts for the water–gas shift reaction: Active phases and reaction intermediates, J. Catal. 291 (2012) 117–126.
[60] S. Chen, A.M. Abdel-Mageed, M. Dyballa, M. Parlinska-Wojtan, J. Bansmann, S. Pollastri, L. Olivi, G. Aquilanti, R.J. Behm, Raising the CO_x methanation activity of a Ru/γ-Al_2O_3 catalyst by activated modification of metal–support interactions, Angew. Chem. Int. Ed. 59 (2020) 22763–22770.
[61] S. Khoobiar, Particle to particle migration of hydrogen atoms on platinum—alumina catalysts from particle to neighboring particles, J. Phys. Chem. 68 (1964) 411–412.
[62] B. Lin, Y. Wu, B. Fang, C. Li, J. Ni, X. Wang, J. Lin, L. Jiang, Ru surface density effect on ammonia synthesis activity and hydrogen poisoning of ceria–supported Ru catalysts, Chin. J. Catal. 42 (2021) 1712–1723.
[63] F. Yang, D. Liu, Y. Zhao, H. Wang, J. Han, Q. Ge, X. Zhu, Size dependence of vapor phase hydrodeoxygenation of m-Cresol on Ni/SiO_2 catalysts, ACS Catal. 8 (2018) 1672–1682.
[64] B. Fang, F. Liu, C. Zhang, C. Li, J. Ni, X. Wang, J. Lin, B. Lin, L. Jiang, Sacrificial sucrose strategy achieved enhancement of ammonia synthesis activity over a ceria–supported Ru catalyst, ACS Sustain. Chem. Eng. 9 (2021) 8962–8969.
[65] Z.-P. Liu, P. Hu, M.-H. Lee, Insight into association reactions on metal surfaces: density-functional theory studies of hydrogenation reactions on Rh(111), J. Chem. Phys. 119 (2003) 6282–6289.
[66] G. Ertl, Reactions at surfaces: from atoms to complexity (nobel lecture), Angew. Chem. Int. Ed. 47 (2008) 3524–3535.
[67] H. Duan, J.-C. Liu, M. Xu, Y. Zhao, X.-L. Ma, J. Dong, X. Zheng, J. Zheng, C.S. Allen, M. Danaie, Y.-K. Peng, T. Issariyakul, D. Chen, A.I. Kirkland, J.-C. Buffet, J. Li, S.C. E. Tsang, D. O'Hare, Molecular nitrogen promotes catalytic hydrodeoxygenation, Nat. Catal. 2 (2019) 1078–1087.
[68] M. Kitano, S. Kanbara, Y. Inoue, N. Kuganathan, P.V. Sushko, T. Yokoyama, M. Hara, H. Hosono, Electride support boosts nitrogen dissociation over ruthenium catalyst and shifts the bottleneck in ammonia synthesis, Nat. Commun. 6 (2015) 6731.
[69] K. Aika, K. Tamaru, Ammonia synthesis over non-iron catalysts and related phenomena, in: A. Nielsen (Ed.), Ammonia: Catalysis and Manufacture, Springer-Verlag, Berlin, 1995, pp. 103–148.